CHAPTER II
LITERATURE REVIEW

2.1 The spin crossover phenomenon

Spin crossover (SCO) is a phenomenon primarily observed in first-row transition metal complexes with a d^4-d^7 electron configuration and an octahedral coordination. (Hayami et al., 2003; Nihei et al., 2007). The shift between high spin (HS) and low spin (LS) states is determined by the respective splitting energy (Δ_{oct}) and electron pairing energy (P) of the system. In a crystal field diagram, the t_{2g} orbitals (lower level) and e_g orbitals (upper level) represent two distinct energy levels. When $\Delta_{oct} > P$, the t_{2g} orbitals are filled before populating the e_g orbitals, resulting in lower paramagnetic or diamagnetic properties, commonly referred to as the low spin state. On the other hand, when $\Delta_{oct} < P$, the electrons preferentially occupy the half-filled t_{2g} orbitals and then populate the e_g orbitals, resulting in a more paramagnetic state known as the high spin state (Martinho et al., 2020). However, in cases where $\Delta_{oct} \approx P$, both the low spin and high spin states are possible. Application of an external stimuli such as pressure, light, and temperature can induce a spin state change (Tsukiashi et al., 2018). This phenomenon is termed spin crossover.

The spin state transition in Fe(III) SCO occurs between the $S = 5/2$ ($^6A_1$) HS state and $S = 1/2$ ($^2T_2$) LS state and differs from Fe(II) in that both spin states are paramagnetic. This difference has a significant impact on the alteration of the Fe-ligand bond lengths during SCO. Typically, the bond length change upon SCO is around 0.10 – 0.13 Å, whereas Fe(II) systems exhibit approximately 0.20 Å bond length change (Hauser, 2013; Nihei et al., 2007; van Koningsbruggen et al., 2004). In the HS species, the coordination bond lengths are longer compared to the LS species. This discrepancy arises from the presence of unpaired electrons in the anti-bonding e_g orbitals in the HS state, while there are no electrons in the e_g orbitals for the LS species (Nihei et al., 2007). This distinction is crucial because the relatively smaller bond length change

between the two spin states makes light-activated Fe(III) SCO systems exceptionally rare. In these systems, the HS state induced by light quickly relaxes to the LS state.

This effect is known as light-induced excited spin state trapping (LIESST) in SCO complexes (Boonprab et al., 2019).

2.2 Measurement techniques

2.1.1 X-ray crystallography

Single crystal X-ray diffraction is a powerful technique employed to precisely determine the three-dimensional atomic structure of crystalline solids and investigate structural changes in complexes. The properties and functions of materials are significantly influenced by their crystal structures. Moreover, crystal structures provide valuable insights into whether a compound is in a HS or LS state, which can be determined by analyzing the metal-ligand bond lengths. This information reveals details about chemical bonding and any disorder present. Consequently, X-ray diffraction techniques find wide application in materials research.

2.1.1.1 Metal-ligand bond length

Changes in metal-ligand bond lengths are utilized to determine if spin crossover has occurred. In Fe(III) systems, the Fe-O/N bond lengths in the LS and HS states are generally 1.85-1.90 / 1.90-1.96 Å and 1.90-1.95 / 2.01-2.22 Å, respectively. These bond length fluctuations are less than those observed in Fe(II) complexes with Fe-N bond lengths of ca. 1.8-2.0 Å in the LS state and ca. 2.0-2.2 Å in the HS state (Díaz-Torres et al., 2020; Phonsri et al., 2017).

2.1.1.2 Distortion in octahedral coordination complexes

The mean metal-ligand distances within the octahedral coordination sphere are measured by d_{mean}, one of the easiest metrics to trace this change. The parameters Σ and Θ have been introduced and utilized to describe angular and torsional distortions, respectively. Σ denotes general deviations from an ideal octahedral structure of the metal ion complex, whereas Θ denotes a distortion from a perfect octahedral (O_h) to a trigonal prismatic (D_{3h}) geometry (Ketkaew et al., 2021). The mathematical formulations of Σ and Θ parameters are expressed through the following equations 2.1 and 2.2 respectively. Descriptions of the angles used to

calculate the distortion indices Σ and Θ for a six-coordinate complex are shown in Figure 2.1 (Halcrow, 2011).

$$\Theta = \sum_{i=1}^{24} |\theta_i - 60| \qquad \textbf{Equation 2.2}$$

$$\Sigma = \sum_{i=1}^{12} |\phi_i - 90| \qquad \textbf{Equation 2.1}$$

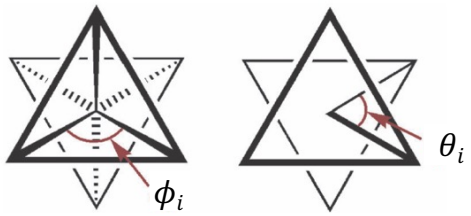

Figure 2.1 Definitions of the angles use to calculate the distortion indices Σ and Θ in a six-coordinate complex.

The parameter Σ is the sum of 12 different *cis* ligand-metal-ligand angles (ϕ_i) that differ from 90 degrees. The parameter Θ quantifies the extent of trigonal distortion in coordination geometry, describing the transition from an octahedral to a trigonal prismatic arrangement. It is calculated as the sum of the deviations of 24 distinct torsional angles (θ_i)—measured between ligand atoms on opposing triangular faces of the octahedron along the pseudo-threefold axis—from the ideal 60°. Nearly two decades ago, Marchivie et al. established the significance of the Θ parameter, demonstrating that variations in Θ between the high-spin (HS) and low-spin (LS) states are correlated with the limiting temperature for photo-inscription, T(LIESST). The values of Σ and Θ for a perfect octahedron are zero in all cases. Recently, Ketkaew *et al.* released OctaDist, a program to calculate these distortion parameters in octahedral complexes (Ketkaew et al., 2021).

2.1.2 SQUID magnetometry

The magnetic profile of a spin crossover (SCO) compound is primarily determined by measuring its magnetic susceptibility ($\chi_M T$) as a function of temperature. The value of $\chi_M T$ is influenced by the temperature-dependent contributions of the high-spin χ_{HS} and low-spin χ_{LS} states. A spin transition occurs when changes in the occupancy of the t_{2g} and e_g orbitals lead to an expansion of the metal-ligand bond length, altering the system's paramagnetic properties. Since the susceptibilities and mole fractions of both spin states can be determined at any given temperature, the spin transition curve can be plotted. Specifically, a graph of the high-spin fraction (γ_{HS}) versus temperature illustrates the progression of the transition (Clarke et al., 2004).

Several characteristic types of spin transition curves exist, as shown in Figure 2.2: (a) abrupt transitions, which exhibit strong cooperativity and are suitable for switching applications; (b) gradual transitions, where cooperative interactions are weak; (c) multi-step transitions, in which a molecule transitions from a binary to a ternary or higher-order switch; (d) abrupt spin crossover with hysteresis, applicable in memory devices; and (e) incomplete transitions. An abrupt spin transition with hysteresis is a key example of bistability, indicating strong cooperative interactions within the material (Clarke et al., 2004; Martinho et al., 2020)

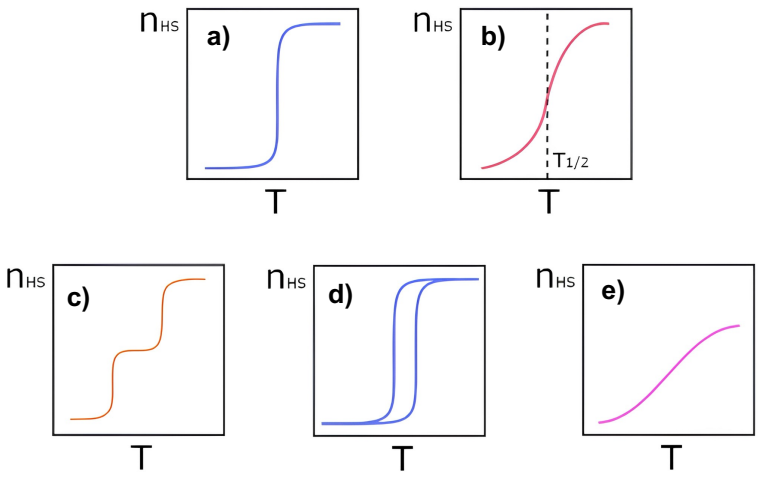

Figure 2.2 Different types of spin crossover profiles.

2.3 Supramolecular Interactions

Components in the lattice, such as solvents, host molecules, and counter ions, play a significant role in controlling the characteristics of the interactions between metal centers and the extent of communication among them. The properties and arrangement of the ligands play a crucial role in enhancing interactions between metal centers. The capacity to form intermolecular interactions is nearly as important as possessing the appropriate ligand-field strength to modulate the balance between Δ_{oct} and P. When the compounds are ionic, the strongest intermolecular interactions will be electrostatic. Hydrogen bonds between ligands and host molecules or solvates can range from the classic, involving the more electronegative elements, to the weak, where C-H is a ubiquitous donor. Specific functional groups may enhance π-π and C-H$\cdots\pi$ interactions (Calhorda et al., 2013), and the presence of halogens can potentially lead to the formation of halogen bonds (G. R. Desiraju et al., 2013). Although some of these interactions may seem quite weak, cooperative effects in the solid state can significantly enhance their importance. For example, the incorporation of a cationic Fe(III) complex into a halogen-bonded supramolecular framework has been shown to influence spin crossover (Jeon et al., 2017).

2.3.1 Hydrogen bonding

The hydrogen bond is the interaction between a hydrogen atom (hydrogen bond donor) commonly attached to N, O, or F and another atom with unshared electrons (hydrogen bond acceptor), denoted as D-H. D-H is a proton donor to A in this interaction. A normal hydrogen bond has only one acceptor and is classified as either linear or bent depending on the angle of D-H$\cdots$A. However, bifurcated, and trifurcated hydrogen bonds are other common types of hydrogen interactions (Figure 2.3). There are two or three donors or acceptors in a bifurcated or trifurcated hydrogen bond.

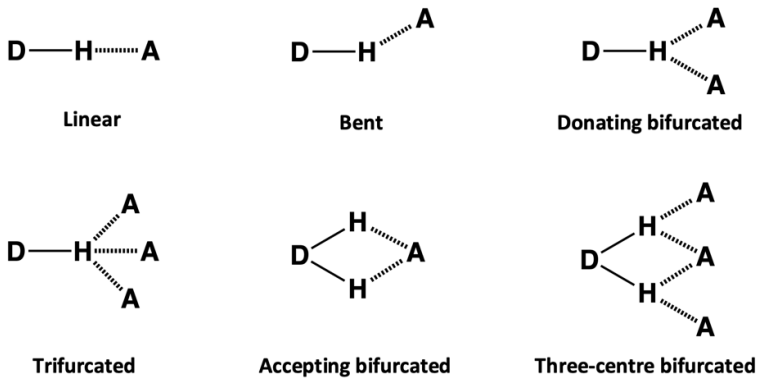

Figure 2.3 Types of hydrogen bonding.

The distance between the donor and acceptor atoms (H···A and D···A) as well as the angle (D-H···A) can be used to investigate the strength of a hydrogen bond. The distance between H···A should be shorter than the van der Waals radii, and the angle should be near to 180° (G. Desiraju, 2005) as shown in Table 2.1.

Table 2.1 The guiding criteria for classifying the strength of hydrogen bonding interactions.

Interaction	Strong	Moderate	Weak
Interaction type	Strongly covalent	Mainly electrostatic	Electrostatic
Bond energy (kJ mol^{-1})	60-120	16-60	<12
Bond length (Å)			
H···A	1.2-1.5	1.5-2.2	2.2-3.2
D···A	2.2-2.5	2.5-3.2	3.2-4.0
Bond angle (°)	175-180	130-180	90-150

2.3.2 Halogen bonding

When a halogen atom forms a covalent bond with another element, such as in a carbon–halogen (C–X) bond, it develops a distinctive electrostatic potential distribution. This includes a positively charged polar cap, known as a **σ-**hole, and a negatively charged equatorial belt. The **σ-**hole serves as an electrophilic site

that can interact with nucleophiles, while the electron-rich equatorial belt can engage with electrophiles from other molecules.

In 2013, the International Union of Pure and Applied Chemistry (IUPAC) defined halogen bonding as “a halogen bond is formed when a halogen atom’s electrophilic region interacts attractively with a nucleophilic region within the same or a different molecular entity” (G. R. Desiraju et al., 2013). Figure 2.4 presents a representative scheme illustrating a halogen bond.

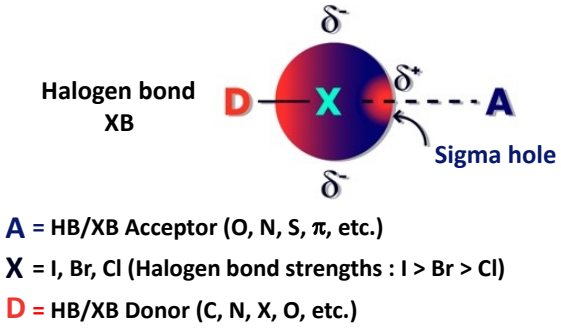

Figure 2.4 A typical scheme for a halogen bond.

2.3.3 π-π and C-H···π interactions

Aromatic interactions involving π-π, cation-π, and anion-π interactions are commonly seen in molecular complexes. π-π interactions typically have an interplanar distance in the range of 3.3-3.8 Å. The aromatic rings can be arranged parallel in either face-to-face or an offset arrangement, Figure 2.5(a) and Figure 2.5(b), respectively. However, when the aromatic planes are perpendicular, a C-H···π interaction is observed Figure 2.5(c) (Molčanov et al., 2019).

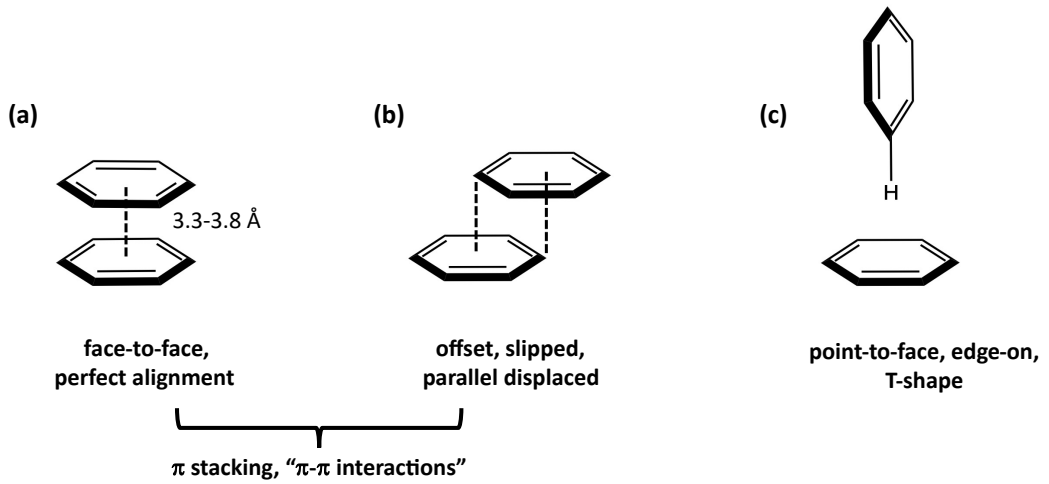

Figure 2.5 π-π and C-H···π arrangements: (a) π-π face-to-face, (b) π-π offset and (c) C-H···π T-shaped.

Parallel fourfold aryl embraces, or P4AE, are made up of one offset face-to-face (OFF) motif and two edge-to-face (EF) motifs that overlap in multiple areas. Therefore, they must have C-H···π and π-π interactions. These are represented diagrammatically in Figure 2.6 (Russell et al., 2001).

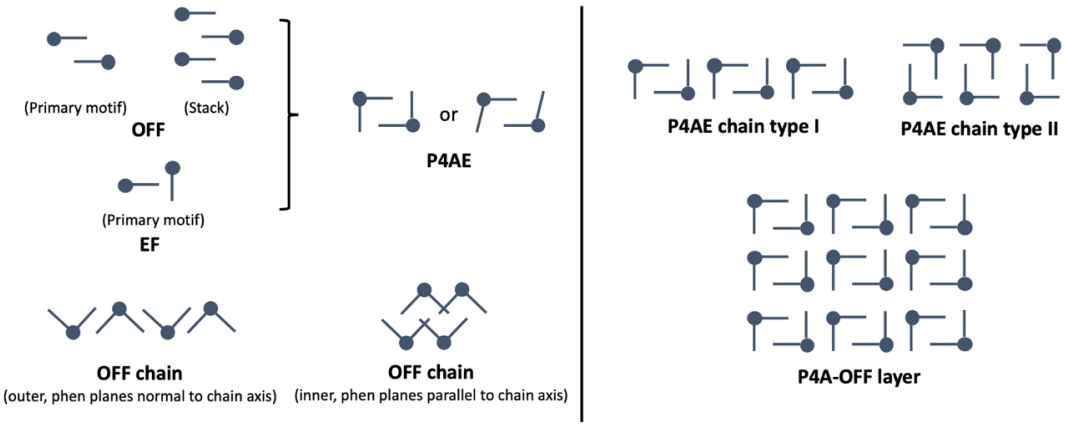

Figure 2.6 Diagrammatic representation of the embraces formed by $[M(phen)_n]^{x+}$ complexes, where the central dot represents the metal center (M), and the lines depict the planes of the phen ligands.

2.4 Spin crossover iron(III)-ethylsalicylaldiminate complexes

2.4.1 SalRen ligands

N-Alkylaminoethylamine and a salicylaldehyde derivative are utilized to synthesize the tridentate ligands known as HsalRen. The NH group on the ligand enhances cooperativity by enabling hydrogen bonding. While various alkyl groups have been previously studied, recent publications predominantly feature ligands containing an ethyl group as shown in Figure 2.7 (Al-Azzani et al., 2020; Sheu et al., 2013). The design of this ligand aims to explore the structural and interaction properties of SCO compounds. Additionally, considerable efforts have been devoted to investigating the impact on SCO characteristics (Harding et al., 2016).

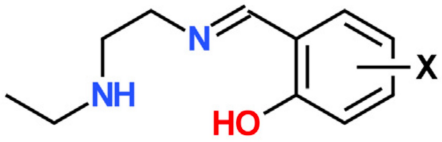

Figure 2.7 Structure of HsalRen-X (R=ethyl group) ligand.

The Hsal-R-en-X ligand family is widely used in SCO research (Dey et al., 2020, 2022, 2023). Compounds containing these ligands exhibit a variety of SCO behaviors, including abrupt SCO in $[Fe(salEen\text{-}3\text{-}OMe)_2]PF_6$ (Haddad et al., 1980, 1981), SCO with an 8 K hysteresis in $[Fe(salEen\text{-}4\text{-}OMe)_2]NO_3$ (Tissot et al., 2014), and near room-temperature SCO in $[Fe(salEen\text{-}3,5\text{-}Br_2)_2]BPh_4$ (Martinho et al., 2014). Structural contractions associated with SCO have been observed in $[Fe(salEen\text{-}4\text{-}Br)_2]ClO_4$ and $[Fe(salEen\text{-}5\text{-}I)_2]ClO_4$ (Bento et al., 2024; Martins et al., 2018; Vicente et al., 2016), resulting in thermosalient properties. While previous studies have primarily focused on the influence of halide substituents, the effect of the anion on these SCO behaviors remains largely unexamined.

2.4.2 Anion effects

The reaction between the salEen ligand and $Fe(ClO_4)_3$ in EtOH resulted in the formation of $[Fe(salEen)_2]ClO_4$ and $[Fe(salEen)_2]ClO_4{\cdot}0.5H_2O$ (Sheu et al., 2013). Both compounds exhibit a gradual SCO behavior, with the non-solvated form displaying a higher $T_{1/2}$ value and a more abrupt SCO transition. Interestingly, the crystal structures of both compounds indicate a slightly greater change in Fe–N/O bond lengths during spin crossover (SCO) for $[Fe(salEen)_2]ClO_4{\cdot}0.5H_2O$. In both structures, the molecular packing is primarily stabilized by strong N–H···anion interactions, which are characteristic of $[Fe(salEen)_2]^+$ complexes. The lack of significant supramolecular interactions accounts for the gradual nature of the SCO in both cases.

Likewise, $[Fe(salEen)_2]_2[Fe(CN)_5(NO)]$ exhibits a gradual SCO between 100 and 400 K (Faulmann et al., 2013), despite having different anions. The packing in the structure remains largely unchanged compared to $[Fe(salEen)_2]ClO_4{\cdot}sol$, resulting in weak connections between the cationic units but strong cation-anion interactions. $[Fe(salEen\text{-}3\text{-}OMe)_2]PF_6$ was synthesized, and magnetic studies indicate a highly abrupt SCO transition at approximately 165 K with a hysteresis of 3 K (Tissot et al., 2011). The structures of the complex at 300 K, 200 K, and 100 K reveal a HS Fe(III) center, HS Fe(III) center, and LS Fe(III) center, respectively. The average change in Fe-N/O bond lengths is around 0.13 Å, which is slightly larger than found in other $[Fe(salEen)_2]^+$ complexes.

The related complexes, $[Fe(salEen\text{-}4\text{-}OMe)_2]Y$ ($Y = NO_3^-$, PF_6^-), when the anion is NO_3^- the SCO is abrupt at approximately 78 K, with a hysteresis of 7.5 K (Tissot et al., 2014). Structural studies confirm the presence of SCO in both compounds. Interestingly, $[Fe(salEen\text{-}4\text{-}OMe)_2]PF_6$ exhibits two independent Fe(III) centers, whereas $[Fe(salEen\text{-}4\text{-}OMe)_2]NO_3$ contains a single Fe(III) center. In $[Fe(salEen\text{-}4\text{-}OMe)_2]NO_3$, a 2D supramolecular network is formed through a combination of N-H···O and C-H···O interactions involving the NO_3 anions (Figure 2.8). Conversely, $[Fe(salEen\text{-}4\text{-}OMe)_2]PF_6$ displays very weak contacts between the cations, resulting in two centers that undergo SCO at identical temperatures, leading to a gradual SCO.

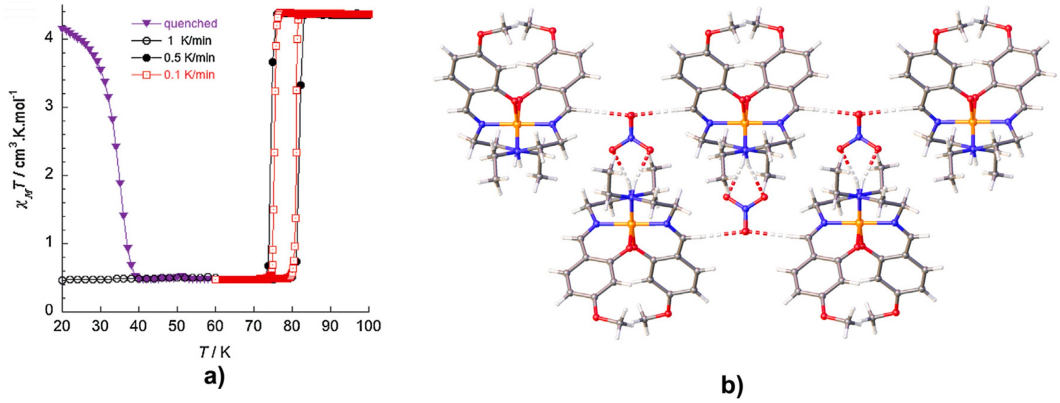

Figure 2.8 (a) The magnetic profile and (b) Packing in $[Fe(salEen\text{-}4\text{-}OMe)_2]NO_3$ showing the 2D supramolecular network (Harding et al., 2016).

Harding et al. recently published a series of three structurally identical Fe(III) complexes, $[Fe(salEen\text{-}5\text{-}I)_2]$halide (Boonprab et al., 2024) where the absence of lattice solvents enables a direct comparison of their properties. Their findings indicate that larger anions are more likely to stabilize the LS state. Notably, $[Fe(salEen\text{-}5\text{-}I)_2]Br$ exhibits a stepped SCO transition near room temperature around 288 K, while $[Fe(salEen\text{-}5\text{-}I)_2]Cl$ and $[Fe(salEen\text{-}5\text{-}I)_2]I$ display gradual and incomplete SCO transitions over a broad temperature range over 200 K (Figure 2.11). Structural analysis shows that N–H···anion and C–H···anion interactions link the cations into two-dimensional Diamond-shaped sheets (Figure 2.9). By employing structural parameters A–C (Figure 2.10) to characterize nearest and next-nearest neighbor interactions, the abruptness and stepped nature of the SCO transition in $[Fe(salEen\text{-}5\text{-}I)_2]Br$ can be rationalized. Comparisons with related complexes, such as $[Fe(salEen\text{-}5\text{-}Br)_2]ClO_4$ and $[Fe(salEen\text{-}5\text{-}I)_2]ClO_4$ (Martins et al., 2018; Vicente et al., 2016), suggest that this magnetic-structural correlation extends to a wider range within this family of compounds.

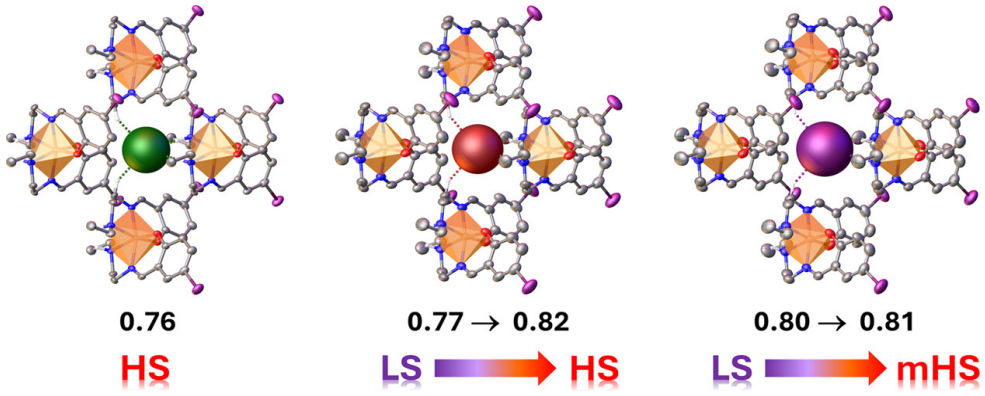

Figure 2.9 Space-filling packing of [Fe(salEen-5-I)$_2$]halide; Cl^- (left), Br^- (center), and I^- (right) viewed along the c-axis in the HS state, showing changes in normalized N–H···anion contacts during spin crossover (Boonprab et al., 2024).

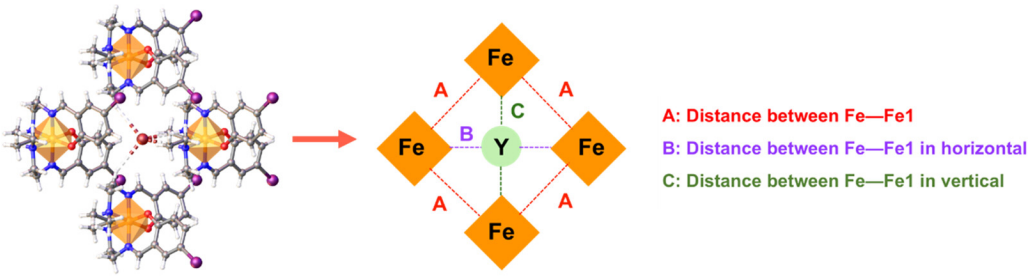

Figure 2.10 A simplified representation of [Fe(salEen-5-I)$_2$]halide viewed along the c-axis, highlights three key structural parameters: A, B, and C (Boonprab et al., 2024).

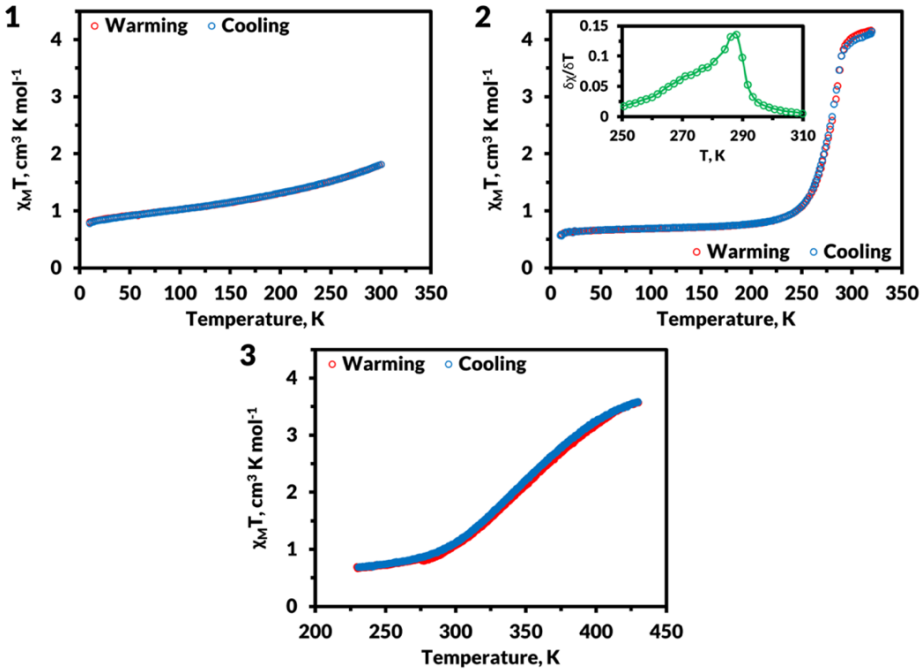

Figure 2.11 Magnetic susceptibility in the solid state (cm^3 K mol^{-1}) vs. temperature (K) for $[Fe(salEen\text{-}5\text{-}I)_2]$halide; Cl^- (1), Br^- (2), and I^- (3) (Boonprab et al., 2024).

The magnetic behavior of Fe(III) complexes undergoes changes when different anions are present. However, only a limited number of anions have been extensively studied, including NCS, ClO_4, PF_6 and BPh_4. Moreover, there are only a few systematic studies focusing on the effects of varying anions. Within the $[Fe(qsal\text{-}5\text{-}OMe)_2]Y$ {qsal = N-(8-quinolyl)salicylaldimine} system, LS complexes are produced with small anions, while intermediate sized anions induce SCO behavior (Sertphon et al., 2013). Conversely, in the case of $[Fe(Him)_2(hapen)]^+$ complexes, HS behavior is observed with small anions, whereas SCO active systems are associated with intermediate to large anions (Koike et al., 2013). These examples highlight that there is no universal rule governing the promotion of SCO by specific anions, as each ligand system exhibits unique characteristics influenced by factors such as the shape, size, and supramolecular preferences of the anions. In most cases, these factors significantly alter the crystal lattice, thereby impacting the SCO behavior. Consequently, the influence of anions on SCO characteristics is less predictable compared to the effects of solvents (Harding et al., 2016).

2.4.3 Solvent effects

In some cases, the selection of solvent is a key factor in influencing SCO properties. For instance, Martinho *et al*. recently investigated the SCO behavior of [Fe(3,5-Br_2-salEen)$_2$]Y·sol (Y = ClO_4, sol = EtOH; Y = BPh_4, sol = DMF) (Martinho et al., 2014). When the anion is BPh_4, the compound exhibits a very gradual and incomplete SCO, whereas the ClO_4 complex remains in the LS state up to 350 K. The structure of [Fe(3,5-Br_2-salEen)$_2$]BPh_4·DMF at 150 K shows that the Fe(III) center is in the LS state, and unlike other [Fe(X-salEen)$_2$]$^+$ complexes, there are no anion-N-H interactions. Instead, hydrogen bonding occurs between the NH groups and the DMF carbonyl oxygen atom. This significantly reduces cooperativity as the DMF molecule is no longer involved in any supramolecular interactions, aligning with the gradual SCO behavior observed in this compound.

A related series of [Fe(naphBzen)$_2$]halide complexes, specifically [Fe(naphBzen)$_2$]Cl and [Fe(naphBzen)$_2$]Br (Habarakada et al., 2022), demonstrates that different solvates can be obtained through recrystallization from various solvents. Solvent selection is a key factor in determining the spin state of Fe(III) complexes. For example, the hexane solvates exhibit SCO behavior (Figure 2.12), whereas $CHCl_3$ solvates and nonsolvated systems remain in a LS state at elevated temperatures (Figure 2.13). This highlights the significant influence of solvent interactions in stabilizing specific spin states. A notable aspect of the structures is the shorter N–H···halide interactions observed in the $CHCl_3$ and nonsolvated systems. The results suggest a minimum interaction distance of approximately 2.26 Å for Cl^- and 2.43 Å for Br^- below which SCO does not occur. Furthermore, it is evident that an increase in anion size from chloride to iodide leads to a stronger preference for the HS state. Interestingly, SCO behavior is observed exclusively in the hexane solvates, implying that even the weak interactions characteristic of nonpolar solvents can influence SCO properties. Whether this effect is applicable to other SCO systems remains an open question.

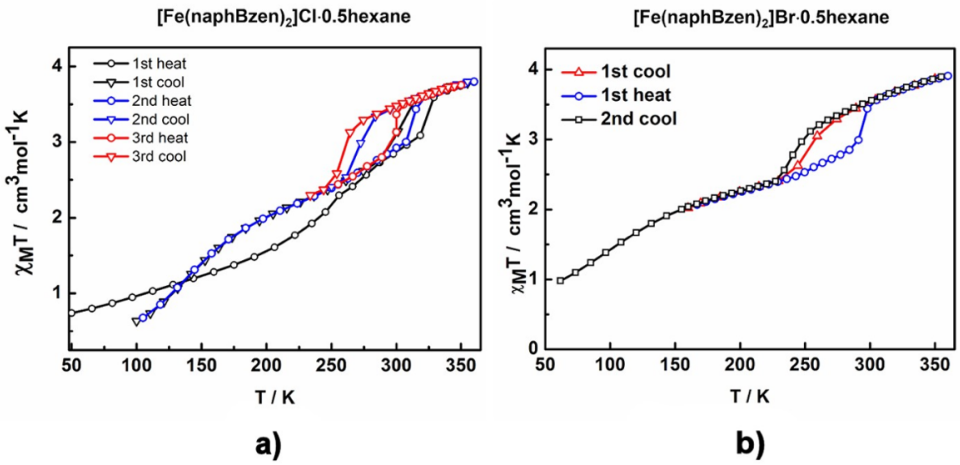

Figure 2.12 Magnetic profiles of [Fe(naphBzen)anion: (a) Cl·0.5hexane and (b) Br·0.5hexane (Habarakada et al., 2022).

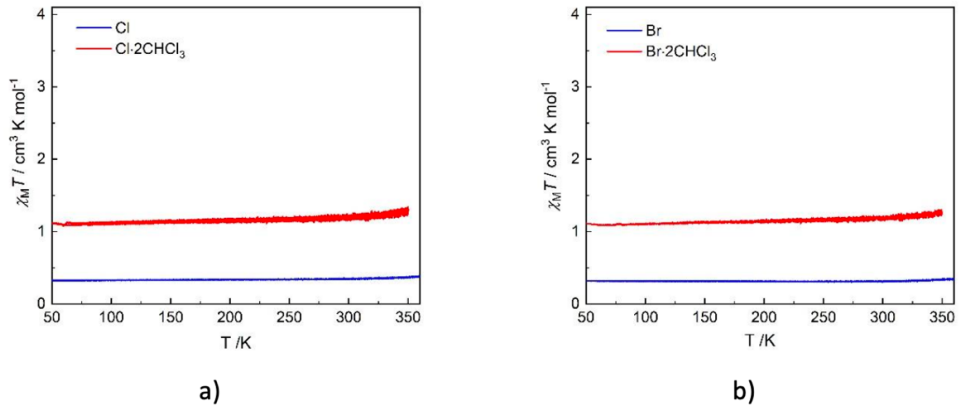

Figure 2.13 VSM $\chi_M T$ vs. T plot of [Fe(naphBzen)$_2$]halide where halide = (a) Cl and (b) = Br from 50-350 K (Habarakada et al., 2022).

2.5 References

Al-Azzani, M. A., Al-Mjeni, F., Mitsuhashi, R., Mikuriya, M., Al-Omari, I. A., Robertson, C. C., Bill, E., and Shongwe, M. S. (2020). Unusual Magneto-Structural Features of the Halo-Substituted Materials [FeIII(5-X-salMeen)$_2$]Y: a Cooperative [HS-HS]<->[HS-LS] Spin Transition. *Chemistry – A European Journal*, *26*(21), 4766–4779. doi: https://doi.org/10.1002/chem.201904744

Bento, M. A., Gomes, T., Martins, F. F., Gil, A., Ferreira, L. P., Barroso, S., Gomes, C. S. B., Garcia, Y., and Martinho, P. N. (2024). The role of intermolecular interactions in [Fe(X-salEen)$_2$]ClO_4 spin crossover complexes. *Dalton Trans.*, *53*(20), 8791–8802. doi: 10.1039/D4DT00400K

Boonprab, T., Lee, S. J., Telfer, S. G., Murray, K. S., Phonsri, W., Chastanet, G., Collet, E., Trzop, E., Jameson, G. N. L., Harding, P., and Harding, D. J. (2019). The First Observation of Hidden Hysteresis in an Iron(III) Spin-Crossover Complex. *Angewandte Chemie International Edition*, *58*(34), 11811–11815. doi: https://doi.org/10.1002/anie.201907619

Boonprab, T., Thammasangwan, W., Chastanet, G., Gonidec, M., Harding, P., and Harding, D. J. (2024). Halide Anion Effects and Magnetostructural Relationships in Iron(III) Spin Crossover Complexes. *Crystal Growth & Design*, *24*, 8145-8152. doi: 10.1021/acs.cgd.4c01068.

Calhorda, M. J., and Costa, P. (2013). Weak Hydrogen Bonding. *Comprehensive Inorganic Chemistry II (Second Edition): From Elements to Applications*, *9*, 341–357. doi: 10.1016/B978-0-08-097774-4.00912-8

Clarke, J., and Braginski, A. I. (2004). *The SQUID Handbook Vol. I The SQUID Handbook* (Vol. 1). Retrieved from http://dnb.ddb.de

Desiraju, G. (2005). The Supramolecular Synthon in Crystal Engineering. In Stimulating Concepts in Chemistry (pp. 293–306). doi: 10.1002/3527605746.ch19

Desiraju, G. R., Ho, P. S., Kloo, L., Legon, A. C., Marquardt, R., Metrangolo, P., Politzer, P., Resnati, G., and Rissanen, K. (2013). Definition of the halogen bond (IUPAC Recommendations 2013): *Pure and Applied Chemistry*, *85*(8), 1711–1713. doi: doi:10.1351/PAC-REC-12-05-10

Dey, B., Cirera, J., Mehta, S., Ferreira, L. P., Arumugam, R., Mondal, A., Martinho, P. N., and Chandrasekhar, V. (2023). Steric Effects on Spin States in a Series of Fe(III) Complexes. *Crystal Growth & Design*, *23*(9), 6668–6678. doi: 10.1021/acs.cgd.3c00555

Dey, B., Gupta, A., Kapurwan, S., and Konar, S. (2020). Study of Spin Crossover Property of a Series of X-OMe-SalEen (X=6, 5 and 4) Based Fe(III) Complexes. *ChemistrySelect*, *5*(46), 14677–14684. doi: https://doi.org/10.1002/slct.202003135

Dey, B., Mehta, S., Mondal, A., Cirera, J., Colacio, E., and Chandrasekhar, V. (2022). Push and Pull Effect of Methoxy and Nitro Groups Modifies the Spin-State Switching Temperature in Fe(III) Complexes. *ACS Omega*, *7*(43), 39268–39279. doi: 10.1021/acsomega.2c05380

Díaz-Torres, R., Phonsri, W., Murray, K. S., Liu, L., Ahmed, M., Neville, S. M., Harding, P., and Harding, D. J. (2020). Spin Crossover in Iron(III) Quinolylsalicylaldiminates: The Curious Case of [Fe(qsal-F)$_2$](Anion). *Inorganic Chemistry*, *59*(18), 13784–13791. doi: 10.1021/acs.inorgchem.0c02201

Faulmann, C., Chahine, J., Valade, L., Chastanet, G., Létard, J.-F., and de Caro, D. (2013). Photomagnetic Studies of Spin-Crossover-and Photochromic-Based Complexes. *European Journal of Inorganic Chemistry*, *2013*(5–6), 1058–1067. doi: https://doi.org/10.1002/ejic.201201328

Habarakada, U., Boonprab, T., Harding, P., S. Murray, K., Phonsri, W., M. Neville, S., Ahmed, M., and J. Harding, D. (2022). Solvent Effects on the Structural and Magnetic Properties of FeIII Spin-Crossover Complexes. *Crystal Growth & Design*, *22*(8), 4895–4905. doi: 10.1021/acs.cgd.2c00390

Haddad, M. S., Federer, W. D., Lynch, M. W., and Hendrickson, D. N. (1980). An explanation of unusual properties of spin-crossover ferric complexes. *Journal of the American Chemical Society*, *102*(4), 1468–1470. doi: 10.1021/ja00524a065

Haddad, M. S., Federer, W. D., Lynch, M. W., and Hendrickson, D. N. (1981). Spin-crossover ferric complexes: unusual effects of grinding and doping solids. *Inorganic Chemistry*, *20*(1), 131–139. doi: 10.1021/ic50215a029

Halcrow, M. A. (2011). Structure:function relationships in molecular spin-crossover complexes. *Chem. Soc. Rev.*, *40*(7), 4119–4142. doi: 10.1039/C1CS15046D

Harding, D. J., Harding, P., and Phonsri, W. (2016). Spin crossover in iron(III) complexes. *Coordination Chemistry Reviews*, *313*, 38–61. doi: https://doi.org/10.1016/j.ccr.2016.01.006

Hauser, A. (2013). Spin-Crossover Materials. Properties and Applications. Edited by Malcolm A. Halcrow. *Angewandte Chemie International Edition*, *52*(40), 10419. doi: https://doi.org/10.1002/anie.201306160

Hayami, S., Kawahara, T., Juhasz, G., Kawamura, K., Uehashi, K., Sato, O., and Maeda, Y. (2003). Iron(III) spin transition compound with a large thermal hysteresis. *Journal of Radioanalytical and Nuclear Chemistry*, *255*. doi: 10.1023/A:1022503609539

Jeon, I.-R., Jeannin, O., Clérac, R., Rouzières, M., and Fourmigué, M. (2017). Spin-state modulation of molecular FeIII complexes via inclusion in halogen-bonded supramolecular networks. *Chemical Communications*, *53*(36), 4989–4992. doi: 10.1039/C7CC01943B

Ketkaew, R., Tantirungrotechai, Y., Harding, P., Chastanet, G., Guionneau, P., Marchivie, M., and Harding, D. J. (2021). OctaDist: a tool for calculating distortion parameters in spin crossover and coordination complexes. *Dalton Trans.*, *50*(3), 1086–1096. doi: 10.1039/D0DT03988H

Koike, M., Murakami, K., Fujinami, T., Nishi, K., Matsumoto, N., and Sunatsuki, Y. (2013). Syntheses, three types of hydrogen-bonded assembly structures, and magnetic properties of [FeIII(Him)$_2$(hapen)]Y·solvent (Him=imidazole, hapen=N,N′-bis(2-hydroxyacetophenylidene)ethylenediamine, Y=BPh_4^-, $CF_3SO_3^-$, PF_6^-, ClO_4^-, and BF_4^-). *Inorganica Chimica Acta*, *399*, 185–192. doi: https://doi.org/10.1016/j.ica.2013.01.021

Martinho, P. N., Martins, F. F., Bandeira, N. A. G., and Calhorda, M. J. (2020). *sustainability Spin Crossover in 3D Metal Centers Binding Halide-Containing Ligands: Magnetism, Structure and Computational Studies*. doi: 10.3390/su12062512

Martinho, P. N., Vicente, A. I., Realista, S., Saraiva, M. S., Melato, A. I., Brandão, P., Ferreira, L. P., and De Deus Carvalho, M. (2014). Solution and solid state properties of Fe(III) complexes bearing N-ethyl-N-(2-aminoethyl)salicylaldiminate

ligands. *Journal of Organometallic Chemistry*, *760*, 48–54.
doi: https://doi.org/10.1016/j.jorganchem.2013.12.028

Martins, F. F., Joseph, A., Diogo, H. P., Minas da Piedade, M. E., Ferreira, L. P., Carvalho, M. D., Barroso, S., Romão, M. J., Calhorda, M. J., and Martinho, P. N. (2018). Irreversible Magnetic Behaviour Caused by the Thermosalient Phenomenon in an Iron(III) Spin Crossover Complex. *European Journal of Inorganic Chemistry*, *2018*(25), 2976–2983. doi: https://doi.org/10.1002/ejic.201800605

Molčanov, K., and Kojić-Prodić, B. (2019). Towards understanding **π**-stacking interactions between non-aromatic rings. *IUCrJ*, *6*(2), 156–166.
doi: 10.1107/S2052252519000186

Nihei, M., Shiga, T., Maeda, Y., and Oshio, H. (2007). Spin crossover iron(III) complexes. *Coordination Chemistry Reviews*, *251*(21–24), 2606–2621.
doi: 10.1016/j.ccr.2007.08.007

Phonsri, W., Harding, P., Liu, L., Telfer, S. G., Murray, K. S., Moubaraki, B., Ross, T. M., Jameson, G. N. L., and Harding, D. J. (2017). *Solvent modified spin crossover in an iron(III) complex: phase changes and an exceptionally wide hysteresis †*.
doi: 10.1039/c6sc05317c

Russell, V., Scudder, M., and Dance, I. (2001). The crystal supramolecularity of metal phenanthroline complexes. *J. Chem. Soc.{,} Dalton Trans.*, *6*, 789–799.
doi: 10.1039/B008607J

Sertphon, D., Harding, D. J., Harding, P., Murray, K. S., Moubaraki, B., Cashion, J. D., and Adams, H. (2013). Anionic Tuning of Spin Crossover in Fe ^{III} –Quinolylsalicylal diminate Complexes. *European Journal of Inorganic Chemistry*, *2013*(5–6), 788–795. doi: 10.1002/ejic.201201066

Sheu, C.-F., Chen, S.-M., Lee, G.-H., Liu, Y.-H., Wen, Y.-S., Lee, J.-J., Chuang, Y.-C., and Wang, Y. (2013). Structure and Magnetism of the Iron(III) Spin-Crossover Complex [Fe^{III}{N-ethyl-N-(2-aminoethyl)salicylaldiminate}$_2$]ClO_4. *European Journal of Inorganic Chemistry*, *2013*(5–6), 894–901.
doi: https://doi.org/10.1002/ejic.201201067

Tissot, A., Bertoni, R., Collet, E., Toupet, L., and Boillot, M.-L. (2011). The cooperative spin-state transition of an iron(III) compound [Fe^{III}(3-MeO-SalEen)$_2$]PF_6: thermal-

vs. ultra-fast photo-switching. *Journal of Materials Chemistry*, *21*(45), 18347–18353. doi: 10.1039/C1JM14163E

Tissot, A., Fertey, P., Guillot, R., Briois, V., and Boillot, M.-L. (2014). Structural, Magnetic, and Vibrational Investigations of FeIII Spin-Crossover Compounds [Fe(4-MeO–SalEen)$_2$]X with X = NO_3^- and PF_6^-. *European Journal of Inorganic Chemistry*, *2014*(1), 101–109. doi: https://doi.org/10.1002/ejic.201300960

Tsukiashi, A., Nakaya, M., Kobayashi, F., Ohtani, R., Nakamura, M., M. Harrowfield, J., Kim, Y., and Hayami, S. (2018). Intermolecular Interaction Tuning of Spin-Crossover Iron(III) Complexes with Aromatic Counteranions. *Inorganic Chemistry*, *57*(5), 2834–2842. doi: 10.1021/acs.inorgchem.7b03126

van Koningsbruggen, P. J., Maeda, Y., and Oshio, H. (2004). Spin Crossover in Transition Metal Compounds I. In Iron(III) Spin Crossover Compounds (Vol. 233, pp. 259–324). Springer-Verlag: Berlin, Heidelberg, New York. doi: 10.1007/b95409

Vicente, A. I., Joseph, A., Ferreira, L. P., de Deus Carvalho, M., Rodrigues, V. H. N., Duttine, M., Diogo, H. P., da Piedade, M. E., Calhorda, M. J., and Martinho, P. N. (2016). Dynamic spin interchange in a tridentate Fe(iii) Schiff-base compound. *Chemical Science*, *7*(7), 4251–4258. doi: 10.1039/C5SC04577K